ACS OMEGA

http://pubs.acs.org/journal/acsodf

Article

Electrodeposition of Polyporous Sn−Ni Coating in Deep Eutectic Solvents for Removing Organic Dyes

Jie Nan, Huicong Liu,* Wen Li,* Fuzhen Zhao, Liqun Zhu, Haining Chen,* and Weiping Li*

Cite This: *ACS Omega* 2022, 7, 41013−41020

Read Online

ACCESS | Metrics & More | Article Recommendations | Supporting Information

ABSTRACT: Materials with a high specific surface area including a porous structure have been widely researched due to the applicability in the adsorption of various organic dyes. However, further application of porous materials is limited by the complicated and expensive preparation process. Herein, a Sn−Ni coating with a polyporous structure is successfully prepared via a simple and high-efficiency electrodeposition approach in deep eutectic solvents (DESs). The prepared Sn−Ni coating exhibits a uniform polyporous structure with a diameter of 15 μm. Furthermore, the coating shows excellent adsorption capacity in the removal of acid grain black organic dyestuff. With the rise of preparation temperature from 85 to 105 °C, the electrochemical active surface area and the ratio of nickel increase, which further enhance dye adsorption capacity.

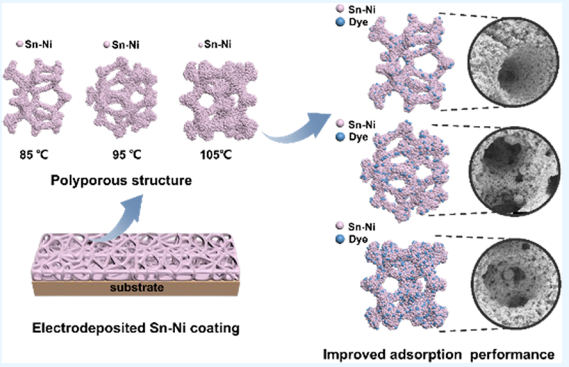

1. INTRODUCTION

With the rapid development of industrialization, organic dyes are widely applied and discharged into water. Simultaneously released dyes are nonbiodegradable and toxic, which could result in water pollution and a great threat to biological health. The research on the removal of dyes from dye-polluted water has captured much attention. Adsorption is one of the most promising methods to treat dye wastewater due to the efficiency, low cost, and sustainability.[1] There are various materials reported to be used as adsorbents, including activated carbon, zeolite,[2] compound biosorption,[3] and porous nanostructure materials. The main research routes for adsorption improvement consist of the construction of high specific surface area structures and the change of surface chemical properties.[4] For activated carbon materials, though they are the most traditional and broadly employed adsorbents, there are limitations to improve the adsorption capacity. Strategies such as oxidation and reduction have been reported to improve absorption capabilities. However, these modification methods would damage the structure and surface of carbon. Meanwhile, the difficulty of separation still blocks the application of carbon adsorbents. Recently, the metal-based adsorbents with properties of the improvement of adsorption capability and the magnetic separation from wastewater have attracted attention. Therefore, metal-based nanostructured adsorbents are considered to be the promising candidates.

Among these metal-based materials, Sn and its alloys play an important role in the applications for removing organic dyes. SnO_2 has been synthesized with different nanostructures including nanosheets, nanoflowers, and porous flower-like structures.[5] It has broad applications in gas sensors and dye adsorption through various nanostructures, such as porous tin dioxide sheets.[6] Meanwhile, Ni could be doped into the metal Sn to change surface properties for the improvement of adsorption.[7,8] With the addition of nickel elements, the performance is improved and the properties are enlarged. Furthermore, doping Ni could cause smaller sizes of nanostructure, and the performance of adsorption has been enhanced.[9] Materials of Ni-doped Sn with high specific surface area nanostructures containing magnetic metal nickel are promising in adsorption.

However, the preparation process of the metal and metal-doped nano/microstructure materials is commonly complicated, expensive, and environmentally unfriendly. Metal−organic frameworks (MOFs) and MOF-derived materials have attracted tremendous attention as excellent candidates in the application of adsorption.[10] MOFs are synthesized usually by a hydrothermal method for more than 12 h,[11−13] even reaching 72 h.[14] After centrifugation and washing, the prepared products still cannot be applied because of its poor stability. Moreover, the synthesis process with carbon or carbonization at high temperatures are common steps before adsorption.[10] Compared to these time-consuming and multistep preparation methods, electrodeposition seems to be a better choice with the merit of easy process and high efficiency.

Received: July 10, 2022
Accepted: October 24, 2022
Published: November 7, 2022

https://doi.org/10.1021/acsomega.2c04354
ACS Omega 2022, 7, 41013−41020

The electrodeposition of tin with conventional aqueous electrolytes is accompanied by a hydrogen evolution reaction.[15−17] The electrodeposition in deep eutectic solvents (DESs) has attracted much attention, and DESs are acknowledged as a promising new form of iconic liquid (ILs) that share many similar properties including wide potential windows, low vapor pressures, no hydrogen evolution reaction, and compositional tunability.[16,18−21]

Herein, this work prepared a Sn−Ni polyporous coating by the electrodeposition approach in DESs with high current density. The coating exhibits a uniform polyporous network structure with a high specific surface area. The addition of nickel and the increase of temperature can change the cathode polarization degree. The Sn−Ni coating of a higher temperature (105 °C) shows outstanding adsorption ability of acid grain black dyestuff.

2. EXPERIMENTAL SECTION

2.1. Materials. The copper substrate was 99% copper with a size of 10 × 40 × 0.3 mm. The tin block and nickel block were of 99% purity and hung by copper wires. The materials for electrodeposition were urea (Macklin, AR, 99%) and choline chloride (Macklin, AR, 99%). The material for copper substrate pretreatment was H_2SO_4(98%) and was diluted to 10%. The materials were purchased from Innochem Co., Ltd.

2.2. Deep Eutectic Solvent Preparation. The electrolyte matrix was first prepared by mixing urea and choline chloride in a molar ratio of 2:1. After stirring at 75 °C for 2 h, the electrolyte matrix was obtained as the solids turned into the mobile phase solvent.

As for the tin deep eutectic solvent, tin and copper listed before were respectively used as anode and cathode. With the current density set as 20 mA·cm^{-2}, the tin anode was dissolved at 105 °C for 1 h in 195 g of the electrolyte matrix. Concentrated hydrochloric acid (15 mL) was added. As for the Sn−Ni deep eutectic solvent, tin and nickel were both used as anode and dissolved at 105 °C with a current density of 30 mA·cm^{-2} for 1 h in 195 g of the electrolyte matrix. The tin and nickel ions came mainly from the dissolution of the anode instead of the salt. Then, moisture was removed by reduced pressure as solvents were heated at 105 °C for 1 h. After the vacuum distillation step, the deep eutectic solvents for electrodeposition were obtained.

As the deposition temperature was set to 105 °C, higher than reported, the electrical conductivity was enough that the salts were not added. Though the high temperature equates to more energy consumption, it is beneficial to the deposition of nickel.

2.3. Morphology and Structure Measurements. The surface morphology of coatings was characterized by scanning electron microscopy (SEM, CAMScan-3400). Energy dispersive spectroscopy (EDS) was applied to investigate the composition and the element ratios of coatings. X-ray photoelectron spectroscopy (XPS, Thermo Escalab 250Xi) was utilized to evaluate the chemical states of compositional elements. X-ray diffraction (XRD, BRUCKER D8 ADVANCE) was used to characterize the crystal structure of deposits. The scan rate and range were 6° per min and 20 to 100°. The morphology and microstructure of coatings were characterized by transmission electron microscopy (TEM, JEM-2100 and JEM-2100F). Two types of sample treatment methods were used before acquiring TEM images. One is scraping off the coating and dispersing in ethanol for 15 min by ultrasound treatment, then dripping on a copper grid. The other one is depositing on an ultra-thin aluminum foil and applying ion-beam milling from the back of the sample. DSC (NETZSCH STA 449 F5/F3 Jupiter) was used for the phase change thermal properties of deposits, set in an Ar atmosphere with a rate of 5 °C per min.

2.4. Electrochemical Characterizations. Electrochemical testing including linear sweep voltammetry (LSV) and cyclic voltammetry (CV) was carried out in a three-electrode electrochemical cell by electrochemical workstations (CH Instruments Ins. CHI440C). LSV was conducted to evaluate the difference between Sn deposition and Sn−Ni co-deposition behaviors.

The three-electrode system used for LSV consisted of a copper substrate electrode, a platinum electrode, and a silver wire as a working electrode, a counter electrode, and a reference electrode. The Sn and Sn−Ni deep eutectic solvents were used as electrolytes. The cathodic polarization curve was characterized at a constant temperature of 85/95/105 °C with a scan rate of 0.005 V·s^{-1}.

CV was conducted to evaluate the specific surface area of coatings. The three-electrode system used for characterizing CV curves consisted of a sample electrode, platinum electrode, and saturated calomel electrode used as a working electrode, counter electrode, and reference electrode. NaCl (3.5%) was selected as the electrolyte.

Adsorption characteristics were determined through a dyestuff color variation test. The organic dyestuff was prepared in the concentration of 1 mg of dyestuff powder in 100 mL of deionized water. The absorbance was measured by a UV−vis spectrophotometer (Shimadzu UV-3600).

3. RESULTS AND DISCUSSION

The main process is presented in Figure 1. The Sn−Ni coating is electrodeposited in DESs at 13.5 A·dm^{-2} for 20 min. A polyporous structure uniformly grows on the copper substrates. Then, the coating is immersed in acid grain black dye. Finally, the organic dyes are removed by the adsorption performance of polyporous coating.

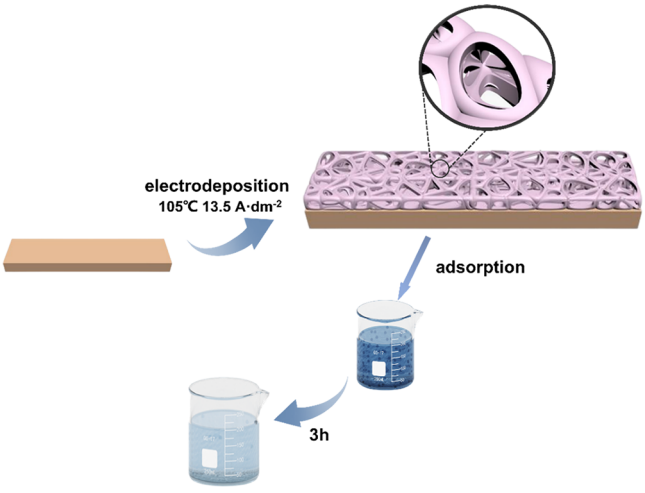

Figure 1. The preparation of Sn−Ni coatings and application for removing organic dyes.

3.1. The Micrographs of Sn−Ni Coatings. The SEM micrographs of Sn and Sn−Ni coatings prepared on copper substrates are shown in Figure 2. The images of Sn coating (Figure 2a,b) consist of bar-shaped particles connected with each other. The compact structure is a typical morphology in

https://doi.org/10.1021/acsomega.2c04354
ACS Omega 2022, 7, 41013−41020

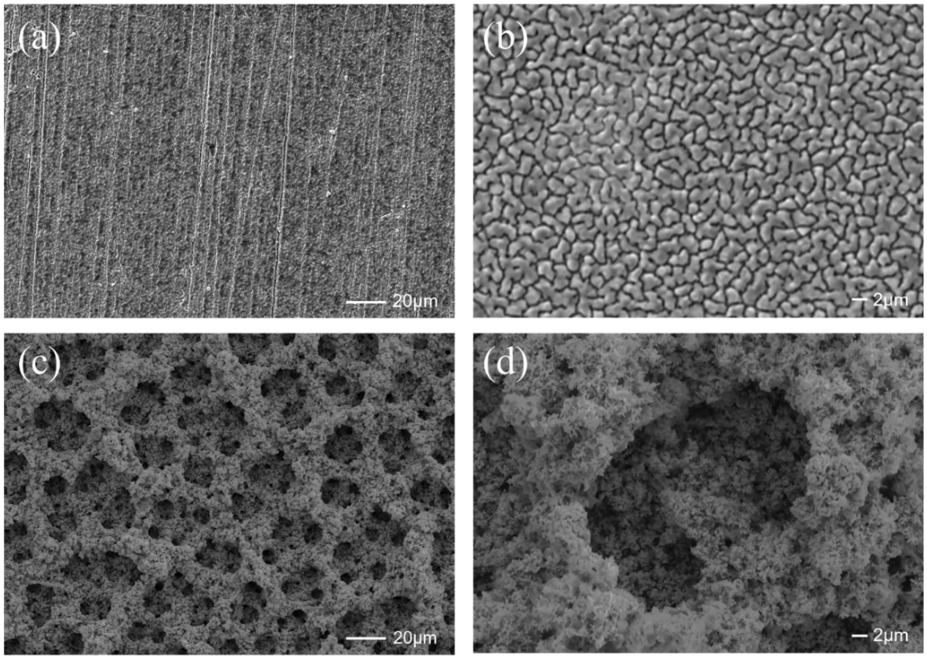

Figure 2. SEM images of (a, b) Sn and (c, d) Sn−Ni coatings.

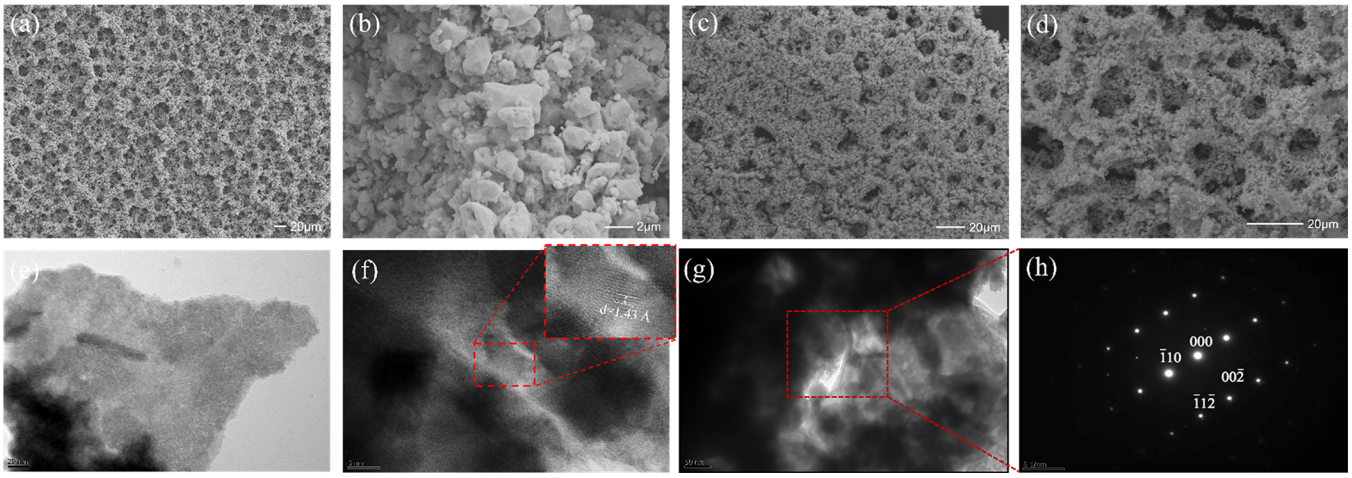

Figure 3. SEM images of Sn−Ni coatings prepared at 105 °C on (a, b) the copper substrate and (c, d) the aluminum foil dissolved by NaOH. (e) TEM image, (f) HRTEM image, and (h) SAED pattern obtained from (g) the selected area of Sn−Ni prepared at 105 °C.

ILM-Sn systems.[20] Compared with the Sn coating prepared at 80 °C, the Sn−Ni coatings could hardly be deposited at the temperature below 85 °C. With the addition of Ni, the structure turns into uniform and small particles. The surface morphologies of Sn−Ni coatings prepared at 85 °C present as uniform porous network structure.

The SEM micrographs of Sn−Ni coatings prepared on copper substrates at 105 °C are exhibited in Figure 3a,b. It can be seen that the structure still appears as a uniform porous network, while the porous network becomes stacked layers. The pore is about 15 μm in diameter. The magnified images (Figure S1a−f) clearly reveal the influence of deposition temperature on the microstructure of particles. As the deposition temperature rises, the pore sizes slightly decrease and the porosity increases. The needlepoint-like particles prepared at 85 °C disappear and switch to stacked lumps.

The coatings were deposited on the aluminum foil at 105 °C and were soaked in 50 g/L NaOH. After the substrate dissolved in NaOH, the relatively complete deposits at different preparation times were observed in the SEM pattern. In the coatings deposited above 10 min (Figure 3c,d), a porous structure had formed. The stripped coatings containing the topside and backside maintained similar structures, which could further demonstrate that the structure of coatings is three dimensional and layer-stacked.

More detailed morphology information of coatings was obtained by TEM and HAADF-STEM techniques. As for the images taken by JEM-2100, the sample scraped from the coating is shown in Figure 3e−h. The sample scraped from the coating and supported on a copper grid is shown to have uniform dot structures in Figure 3e. HRTEM examinations carried out in Figure 3f clearly demonstrate that the crystalline phase grains are distributed in different orientations. The average width of every lattice fringe area is less than 5 nm. The main interplanar spacing is 1.43 Å, corresponding to diffraction spots in Figure 3h. The SAED patterns are shown in the red dotted lined area of Figure

https://doi.org/10.1021/acsomega.2c04354
ACS Omega 2022, 7, 41013−41020

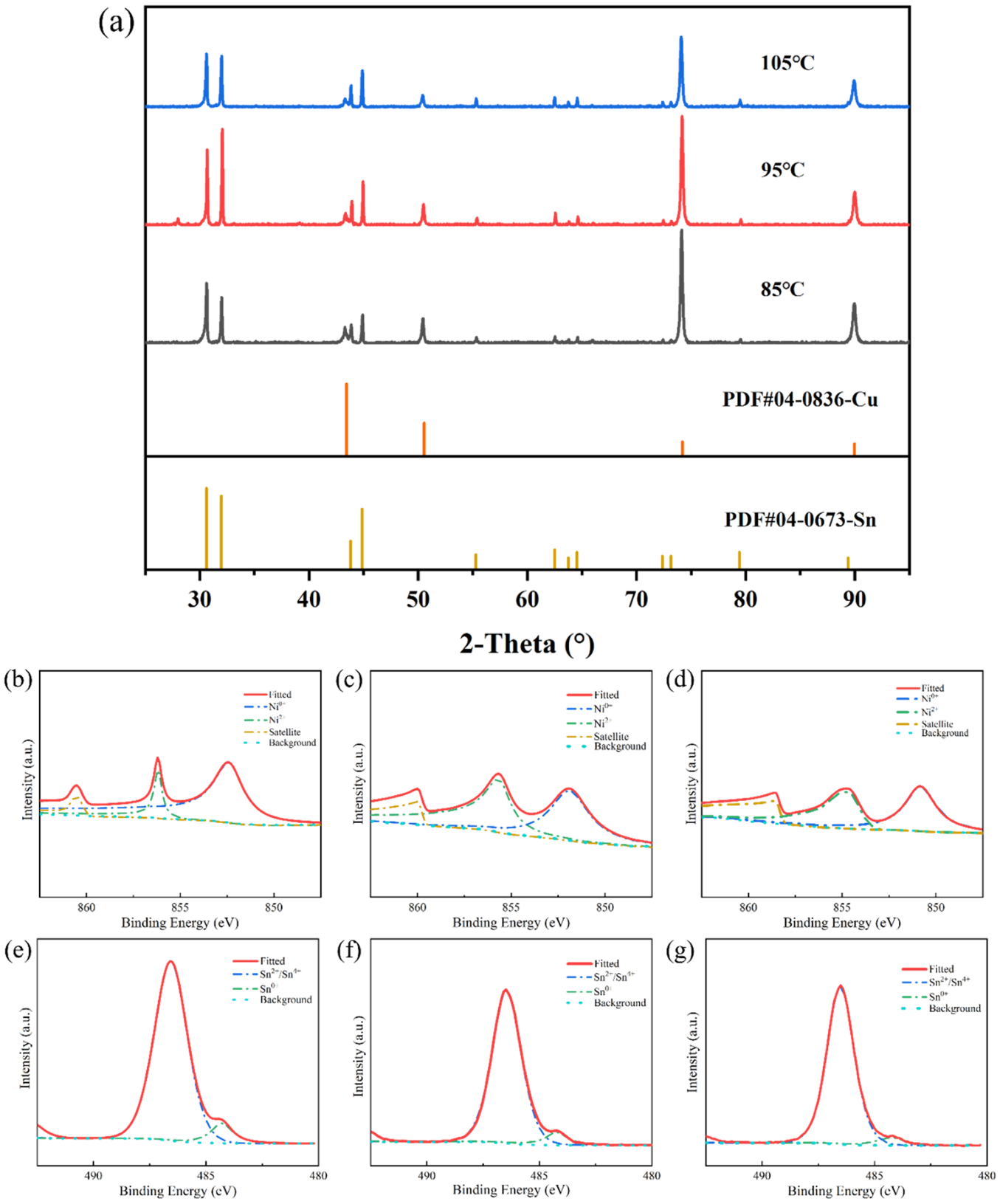

Figure 4. (a) XRD obtained in the Sn−Ni ion deep eutectic solvent at 85/95/105 °C. XPS obtained in the Sn−Ni ion deep eutectic solvents of Ni at (b) 85 °C, (c) 95 °C, and (d)105 °C and Sn at (e) 85 °C, (f) 95 °C, and (g) 105 °C.

3g. The clear and sharp diffraction spots indicate that the selected area is a single-crystalline structure. Through the comparison with the XRD patterns, the coating contains body centered cubic (bcc) tin with [110] zone-axis.

More SAED pattern information is listed in Figure S4. The interplanar spacing is in the range of 2.16 to 3 Å, containing lattice fringes different from those of the pure metallic tin and nickel. The various and different lattice fringes result from the

https://doi.org/10.1021/acsomega.2c04354
ACS Omega 2022, 7, 41013−41020

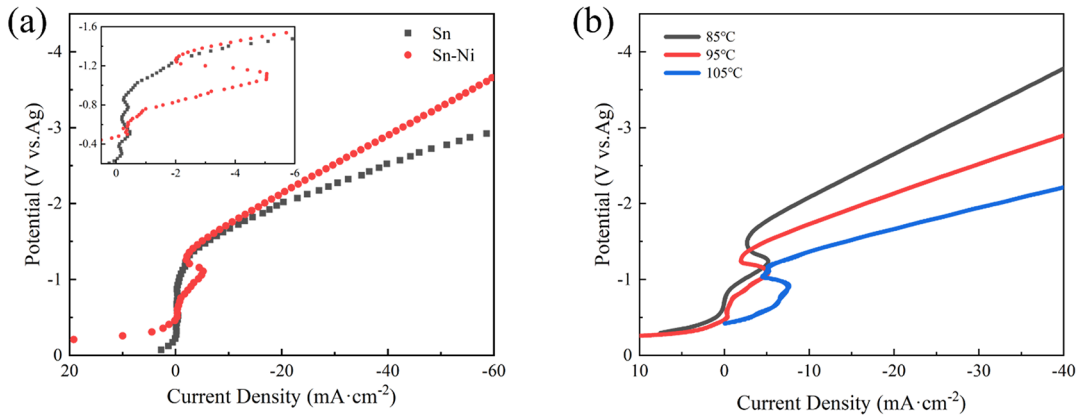

Figure 5. Cathodic polarization curves obtained in (a) the Sn and Sn−Ni ion deep eutectic solvents at 95 °C and (b) the Sn−Ni ion deep eutectic solvent at 85/95/105 °C.

lattice distortion in the Sn−Ni intermetallic compound.[22] The diffraction patterns can reflect the nano-polycrystal structure of coatings.

EDS of the coatings obtained at 85/95/105 °C demonstrates Sn, Ni, and Cu signals, indicating different ratios of tin and nickel elements. The atom percentages of tin and nickel are 95.19% Sn−4.81% Ni at 85 °C, 94.44% Sn−5.56% Ni at 95 °C, and 94.24% Sn−5.76% Ni at 105 °C. It can be seen that with the increase of the preparation temperature, the ratio of nickel to tin increases. The reason for the phenomenon is probably because the increasing temperature improves the growth of nickel instead of tin.

3.2. The Effect of Temperature on the Electrodeposited Coating Structure. The XRD patterns of Sn−Ni coatings prepared at 85/95/105 °C are displayed in Figure 4a. The diffraction peaks in the XRD spectra are indexed to tetragonal Sn (PDF#04-0673) and cubic Cu (PDF#04-0836). The strong diffraction peak from crystalline phases relating to Ni is hardly detected. According to the EDS analysis, the content of Ni is about 5%. On the other hand, Ni is uniformly doped in Sn.

The most distinct differences between the XRD patterns of samples prepared at different temperatures are the intensity of peaks. In the XRD pattern of coatings prepared at 85 °C, the peaks at 30.63, 32.02, 43.87, 44.90, and 79.49° correspond to (2 0 0), (1 0 1), (2 2 0), (2 1 1), and (3 1 2) of Sn. The peaks from 55.31 to 73.195° correspond to (3 0 1), (1 1 2), (4 0 0), (3 2 1), (4 2 0), and (4 1 1) of Sn.

The major peaks are (2 0 0) and (1 0 1) planes with the same intensity. In the XRD pattern of the coating prepared at 95 °C, the intensity of the (2 0 0) peak decreases and the (1 0 1) peak increases. In the XRD pattern of coatings prepared at 105 °C, the major peak turns into (2 0 0). However, the crystal orientation of Sn does not have a regular unidirectional change. The peak corresponding to 79.24°, close to (3 1 2) of tin, appears and becomes sharp as the temperature is increased. The peak corresponding 45.00°, close to (2 1 1) of tin, shifts to the low angle and tends to get fused with the peak (2 1 1). The major peaks like (1 0 1) and (2 0 0) have the same situation.

To analyze the element composition of the prepared coatings, XPS measurements were conducted. The elements of tin and nickel can be detected in the full spectrum analysis. The Ni $2p_{3/2}$ and Sn $3d_{5/2}$ XPS spectra are presented in Figure 5b−g. For the Ni spectrum of prepared coating at 85 °C, the peaks at 852.41 and 856.18 eV could be assigned to Ni^0 and Ni^{2+}, with the broad satellite at 860.53 eV. The peak of Ni^{2+} can be attributed to the generation of NiO in air.[23] As for the spectra of 95 and 105 °C, the peaks of Ni^0 and Ni^{2+} shift toward lower binding energy. It is probably because of the increase of nickel coverage.[24] The intensity change indicates that the NiO/Ni ratio is the lowest at 105 °C. The higher content of active Ni results in better activity.[25]

In the XPS Sn $3d_{5/2}$ spectra of 85 °C, the peaks at 486.57 and 484.30 eV are indexed to the Sn^{x+} and metallic Sn, respectively. With the rise of temperature, the binding energy corresponding to metallic Sn^0 becomes relatively stable (484.24 eV at 95 °C and 484.27 eV at 105 °C), which could probably be the measurement error.

The peak at 486.57 eV can be related to the Sn^{4+} valence state (SnO_2) or Sn^{2+} valence state (SnO). With the increase of temperature, the binding energies corresponding Sn^{4+}/Sn^{2+} decline by about 0.1 eV compared to the peak at 95 °C.

3.3. The Effect of Nickel Ions and Temperature on DESs. The electrochemical measurements were performed to analyze the difference of DESs containing Sn and Sn−Ni. For the electrolyte of tin in Figure 5a, the current density drops from 0.62 to −0.1 mA·cm^{-2} at −0.3 V. The deposition current barely decreases until the overpotential exceeds over 1.2 V. In contrast, the initial polarization current density of Sn−Ni is much higher. The cathodic polarization curve of the electrolyte containing nickel ions reveals a steeper decrease of the current density. In addition, with the overpotential increase from 0.6 to 1.25 V, the current density remains unchanged before the overpotential of 1.0 V and first decreases from −0.1 to −5 mA·cm^{-2} then increases until the overpotential arrives 1.25 V. The peak of the current reversal demonstrates that there is an intermediate reaction process in the electrodeposition of Sn−Ni coating in DESs. The extra reaction hinders the continuous electrodeposition of Sn−Ni, thus causing the pore formation.

The difference of cathodic polarization behavior between the two kinds of deep eutectic solvents shows that the addition of nickel ions has a great impact on the electrochemical properties of the tin ion deep eutectic solvent, hence resulting in the difference of the structure and properties of coatings electrodeposited.

The cathodic polarization curves of the Sn−Ni deep eutectic solvent obtained at 85/95/105 °C are presented in Figure 5b. With the increase of temperature, the cathode current density of the corresponding overpotential increases significantly, and the cathode polarization decreases. It indicates that the increase of temperature results in the reduction of the required deposition

https://doi.org/10.1021/acsomega.2c04354
ACS Omega 2022, 7, 41013−41020

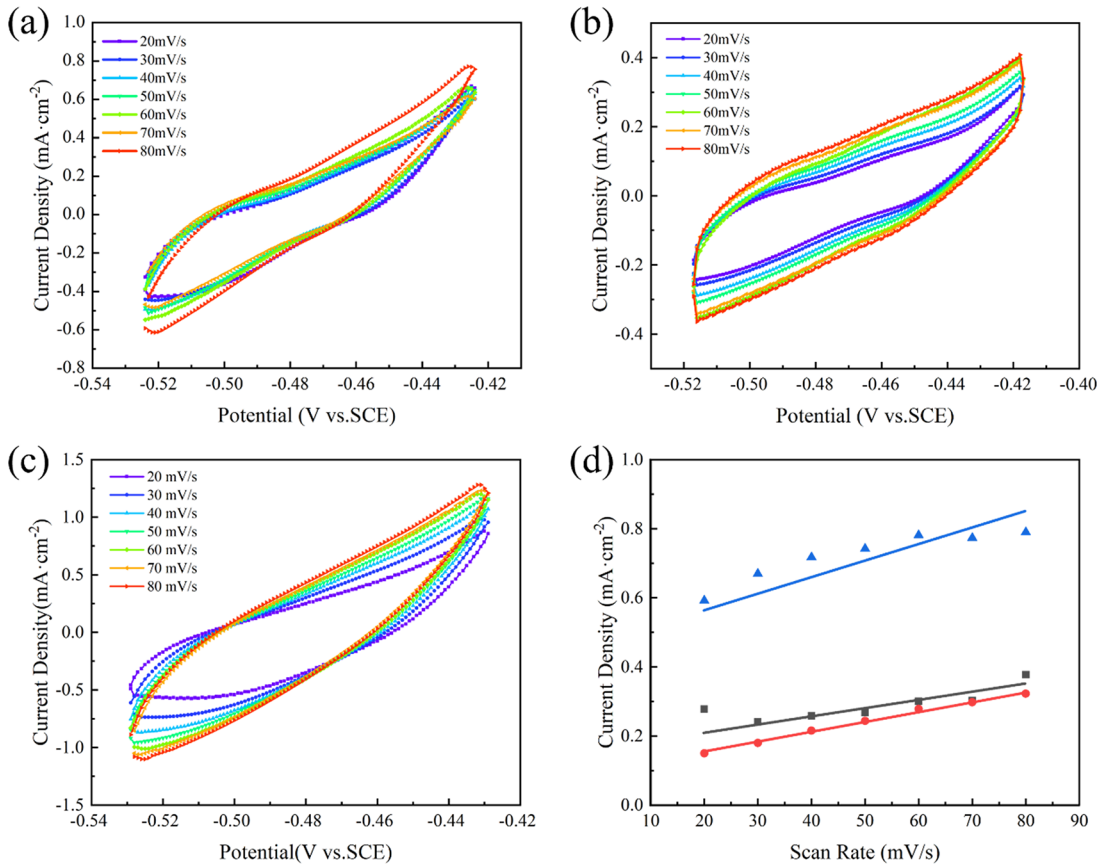

Figure 6. ECSA measurements of Sn−Ni coatings' CV curves and current density differences plotted against scan rates of (a) 85 °C preparation temperature, (b) 95 °C preparation temperature, and (c) 105 °C preparation temperature. (d) Current density plotted against scan rates (105 °C in blue line, 95 °C in red line, and 85 °C in black line).

potential at the same current density. The characteristics of cathodic polarization curves are consistent with the results of EDS.

3.4. The Effect of Temperature on Electrodeposited Coating Performance. Cyclic voltammetry (CV) tests were carried out to measure the electrochemical active surface area (ECSA). The CV curves of the Sn−Ni coatings prepared at 85, 95, and 105 °C are shown in Figure 6. Within the scan rate in the range of 20 to 80 mV/s, the CV curves are enlarged in different degrees.

The double-layer capacitance C_{dl} can be calculated from the slope of the scan rate−current density to compare the specific surface area of coatings. The C_{dl} of the Sn−Ni coatings prepared at 85/95/105 °C is 1.215, 1.455, and 1.545 mF·cm^{-2}. It is clear that the increase of temperature will result in the enlargement of the specific surface area of coatings. Connected with the images of SEM, the phenomenon is reasonable and further demonstrates that the increase of temperature can improve the deposit of the dense porous structure.

On the basis of SEM, the physical models are set in Figure 7a. It can be clearly seen that the coatings deposited at 85 and 95 °C have a similar structure and the immersed acid grain black dyestuff shows similar color changes. By comparison, the coating deposited at 105 °C is composed of denser particles. After 3 h absorption, the dyestuff color becomes lighter, which means better adsorption performance. The SEM images of adsorbed samples prepared at 105 °C show less vacancy between the stacked particles. In addition to the difference of preparation, which is exhibited in the SEM images of primary samples, more dye particles were adsorbed, resulting in the higher density stacked particle structure. Figure 7b further shows the color change and the absorbance of dyestuff immersed by the coatings prepared at 85, 95, and 105 °C. The absorbance reflects the concentration of dyes. The coating prepared at 105 °C exhibits the best performance of the adsorptive removal ability. According to the statistics of pore sizes of samples prepared at 85, 95, and 105 °C in Figure S5, the adsorption effect is presented to be related to the pore sizes.

Adsorption effects of Sn−Ni coatings prepared at 105 °C are exhibited in Figure 7c. To accelerate the adsorption effects, the dyes were heated at 60 °C. The adsorption studies were performed at different contact times (1, 2, and 3 h) as shown in Figure 7c. It can be clearly seen that the decolorization degree increases with the increase of contact time. Therefore, the decolorization phenomenon presents the excellent adsorption capacity of the polyporous Sn−Ni coatings. To further demonstrate the absorption effect of Sn−Ni coating, open circuit potential−time was examined to monitor the potential of the coating prepared at 105 °C in Figure 7d. The potential of the coating immersed in KCO_3 remains constant at −0.98 V, while the potential of the coating immersed in the grain black dyestuff increases continuously. The change might be due to the hydrogen bonds that were formed between N in the molecular chain and active amino of azo dyes and the coating.

4. CONCLUSIONS

In summary, uniform 3D polyporous network structure Sn−Ni coatings have been deposited with high current density in the

https://doi.org/10.1021/acsomega.2c04354
ACS Omega 2022, 7, 41013−41020

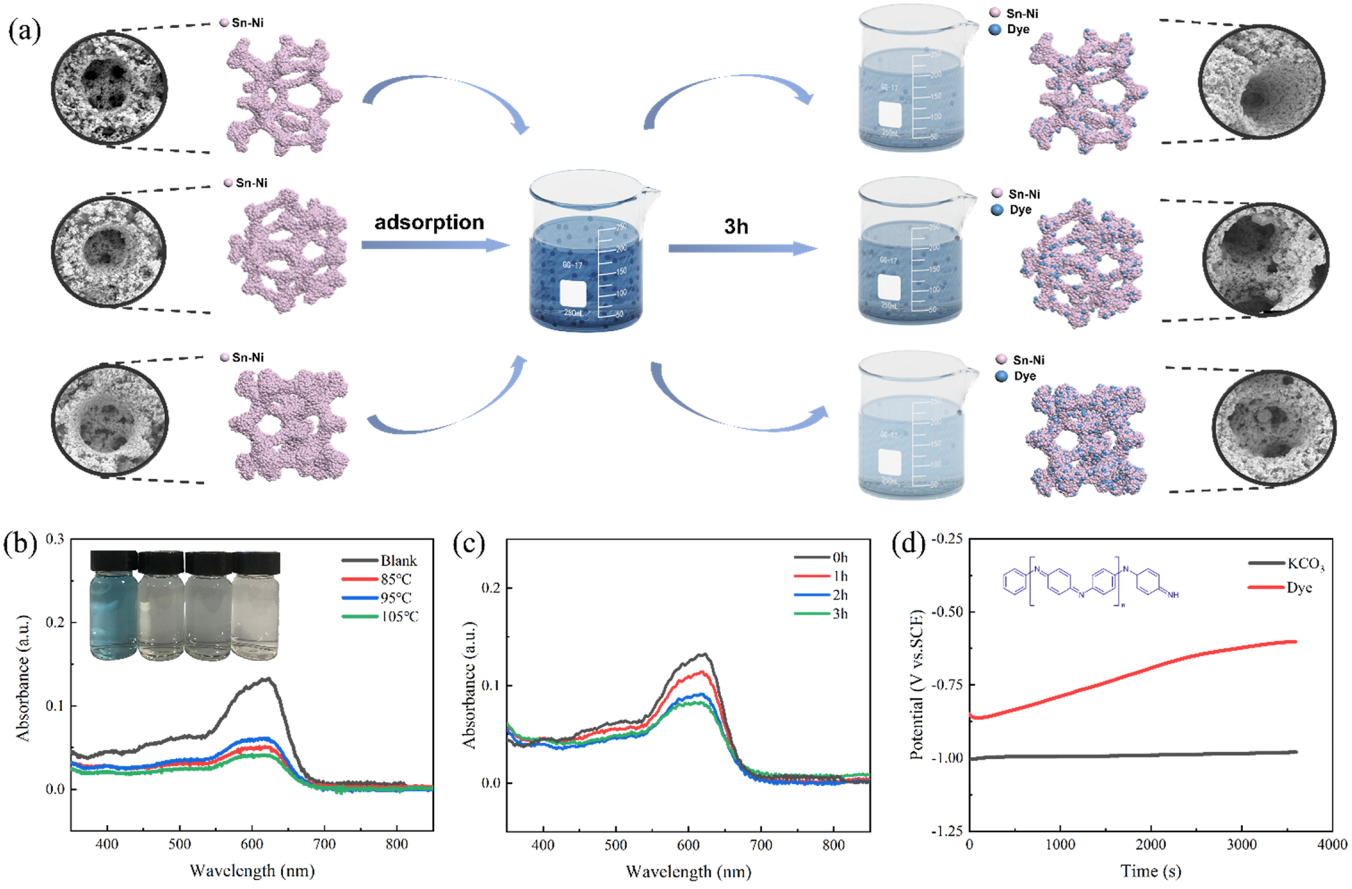

Figure 7. (a) The absorption process of coatings prepared at 85, 95, and 105 °C (from top to bottom). (b) UV−visible spectra of the acid grain black dyestuff after contact with the coatings prepared at 85, 95, and 105 °C (from left to right). (c) UV−visible spectra of the acid grain black dyestuff after contact with the coating at 60 for 0 to 3 h. (d) Open circuit potential−time curve of the coating prepared at 105 °C immersed in KCO_3 and dye.

DESs. The dye adsorption experiments indicated that the prepared Sn−Ni coatings have outstanding adsorption capacity of the acidic grain black dyestuff. Through the comparison of the adsorption effect and CV examination, the coatings at the preparation temperature of 105 °C with more electrochemical active surface area show superior performance in the adsorption of dye. The coatings were composed of 94.24% tin and 5.76% nickel nanoparticles uniformly dispersed. The results offer an insight into the electrodeposition of high specific surface area Sn−Ni coatings in the deep eutectic solvents with promising applications in the dye separation in water.

■ ASSOCIATED CONTENT

Supporting Information

The Supporting Information is available free of charge at https://pubs.acs.org/doi/10.1021/acsomega.2c04354.

Additional SEM images, HRTEM images, SAED patterns, and EDS of Sn−Ni coatings prepared at different condition; statistics of pore sizes (PDF)

■ AUTHOR INFORMATION

Corresponding Authors

Huicong Liu − *School of Materials Science and Engineering, Beihang University, Beijing 100191, China*; Email: liuhc@buaa.edu.cn

Wen Li − *AVIC Manufacturing Technology Institute, Beijing 100024, China*; Email: liwen1013@126.com

Haining Chen − *School of Materials Science and Engineering, Beihang University, Beijing 100191, China*; orcid.org/0000-0002-7543-3674; Email: chenhaining@buaa.edu.cn

Weiping Li − *School of Materials Science and Engineering, Beihang University, Beijing 100191, China*; Email: liweiping@buaa.edu.cn

Authors

Jie Nan − *School of Materials Science and Engineering, Beihang University, Beijing 100191, China*

Fuzhen Zhao − *School of Materials Science and Engineering, Beihang University, Beijing 100191, China*

Liqun Zhu − *School of Materials Science and Engineering, Beihang University, Beijing 100191, China*

Complete contact information is available at: https://pubs.acs.org/10.1021/acsomega.2c04354

Notes

The authors declare no competing financial interest.

■ ACKNOWLEDGMENTS

This work was supported by the National Natural Science Foundation of China (Grant No. 51971012) and Beijing Natural Science Foundation (Grant No. 2214084).

REFERENCES

(1) Yagub, M. T.; Sen, T. K.; Afroze, S.; Ang, H. M. Dye and its removal from aqueous solution by adsorption: A review. *Adv. Colloid Interfaces Sci.* **2014**, *209*, 172−184.

(2) Cheng, Z.-L.; Li, Y.-X.; Liu, Z. Study on adsorption of rhodamine B onto Beta zeolites by tuning SiO2/Al2O3 ratio. *Ecotox. Environ. Safe.* **2018**, *148*, 585−592.

(3) Reghioua, A.; Barkat, D.; Jawad, A. H.; Abdulhameed, A. S.; Khan, M. R. Synthesis of Schiff's base magnetic crosslinked chitosan-glyoxal/ZnO/Fe3O4 nanoparticles for enhanced adsorption of organic dye: Modeling and mechanism study. *Sustainable Chem. Pharm.* **2021**, *20*, No. 100379.

(4) Xiao, W.; Jiang, X.; Liu, X.; Zhou, W.; Garba, Z. N.; Lawan, I.; Wang, L.; Yuan, Z. Adsorption of organic dyes from wastewater by metal-doped porous carbon materials. *J. Cleaner Prod.* **2021**, *284*, No. 124773.

(5) Gattu, K. P.; Ghule, K.; Kashale, A. A.; Patil, V. B.; Phase, D. M.; Mane, R. S.; Han, S. H.; Sharma, R.; Ghule, A. V. Bio-green synthesis of Ni-doped tin oxide nanoparticles and its influence on gas sensing properties. *RSC Adv.* **2015**, *5*, 72849−72856.

(6) Liu, J.; Wan, Y.; Meng, F.; Huang, X.; Liu, J. Novel hierarchically-packed tin dioxide sheets for fast adsorption of organic pollutant in aqueous solution. *J. Mater. Chem.* **2012**, *22*, 2885−2893.

(7) Hu, J.; Yu, H.; Dai, W.; Yan, X.; Hu, X.; Huang, H. Enhanced adsorptive removal of hazardous anionic dye "congo red" by a Ni/Cu mixed-component metal−organic porous material. *RSC Adv.* **2014**, *4*, 35124−35130.

(8) Kim, T.-S.; Song, H. J.; Dar, M. A.; Lee, H.-J.; Kim, D.-W. Fast adsorption kinetics of highly dispersed ultrafine nickel/carbon nanoparticles for organic dye removal. *Appl. Surf. Sci.* **2018**, *439*, 364−370.

(9) Manikandan, V.; Petrila, I.; Vigneselvan, S.; Mane, R. S.; Vasile, B.; Dharmavarapu, R.; Lundgaard, S.; Juodkazis, S.; Chandrasekaran, J. A reliable chemiresistive sensor of nickel-doped tin oxide (Ni-SnO) for sensing carbon dioxide gas and humidity. *RSC Adv.* **2020**, *1*, 3384−3796.

(10) Liu, D.; Gu, W.; Zhou, L.; Wang, L.; Zhang, J.; Liu, Y.; Lei, J. Recent advances in MOF-derived carbon-based nanomaterials for environmental applications in adsorption and catalytic degradation. *Chem. Eng. J.* **2022**, *427*, No. 131503.

(11) Hasanzadeh, M.; Simchi, A.; Shahriyari Far, H. Nanoporous composites of activated carbon-metal organic frameworks for organic dye adsorption: Synthesis, adsorption mechanism and kinetics studies. *J. Ind. Eng. Chem.* **2020**, *81*, 405−414.

(12) Lai, Y.; Wang, F.; Zhang, Y.; Ou, P.; Wu, P.; Fang, Q.; Chen, Z.; Li, S. UiO-66 derived N-doped carbon nanoparticles coated by PANI for simultaneous adsorption and reduction of hexavalent chromium from waste water. *Chem. Eng. J.* **2019**, *378*, No. 122069.

(13) Tsai, F.-C.; Xia, Y.; Ma, N.; Shi, J. J.; Jiang, T.; Chiang, T. C.; Zhang, Z. C.; Tsen, W. C. Adsorptive removal of acid orange 7 from aqueous solution with metal−organic framework material, iron (III) trimesate. *Desalin. Water Treat.* **2016**, *57*, 3218−3226.

(14) Zhao, Y.; Wang, L.; Fan, N.-N.; Han, M.-L.; Yang, G.-P.; Ma, L.-F. Porous Zn(II)-Based Metal−Organic Frameworks Decorated with Carboxylate Groups Exhibiting High Gas Adsorption and Separation of Organic Dyes. *Cryst. Growth Des.* **2018**, *18*, 7114−7121.

(15) Cao, X.; Xu, L.; Wang, C.; Li, S.; Wu, D.; Shi, Y.; Liu, F.; Xue, X. Electrochemical Behavior and Electrodeposition of Sn Coating from Choline Chloride−Urea Deep Eutectic Solvents. *Coatings* **2020**, *10*, 1154.

(16) Alesary, H. F.; Ismail, H. K.; Shiltagh, N. M.; Alattar, R. A.; Ahmed, L. M.; Watkins, M. J.; Ryder, K. S. Effects of additives on the electrodeposition of Zn Sn alloys from choline chloride/ethylene glycol-based deep eutectic solvent. *J. Electroanal. Chem.* **2020**, *874*, 114517.

(17) Salomé, S.; Pereira, N. M.; Ferreira, E. S.; Pereira, C. M.; Silva, A. F. Tin electrodeposition from choline chloride based solvent: Influence of the hydrogen bond donors. *J. Electroanal. Chem.* **2013**, *703*, 80−87.

(18) Abbott, A. P.; Capper, G.; Davies, D. L.; Rasheed, R. K.; Tambyrajah, V. Novel solvent properties of choline chloride/urea mixtures. *Chem. Commun.* **2003**, 70−71.

(19) Cojocaru, A.; Costovici, S.; Anicai, L.; Visan, T. Studies of cathodic processes during NiSn alloy deposition using choline chloride based ionic liquids. *Metal. Int* **2009**, *14*, 1−11.

(20) Anicai, L.; Petica, A.; Costovici, S.; Prioteasa, P.; Visan, T. Electrodeposition of Sn and NiSn alloys coatings using choline chloride based ionic liquids—Evaluation of corrosion behavior. *Electrochim. Acta* **2013**, *114*, 868−877.

(21) Rosoiu, S. P.; Pantazi, A. G.; Petica, A.; Cojocaru, A.; Costovici, S.; Zanella, C.; Visan, T.; Anicai, L.; Enachescu, M. Electrodeposition of NiSn-rGO Composite Coatings from Deep Eutectic Solvents and Their Physicochemical Characterization. *Metals* **2020**, *10*, 1455.

(22) Zhao, H.; Chen, J.; Wei, W.; Ke, S.; Zeng, X.; Chen, D.; Lin, P. Synthesis of Ni@NiSn Composite with High Lithium-Ion Diffusion Coefficient for Fast-Charging Lithium-Ion Batteries. *Global Challenges* **2020**, *4*, 1900073.

(23) Biesinger, M. C.; Payne, B. P.; Grosvenor, A. P.; Lau, L. W. M.; Gerson, A. R.; Smart, R. S. C. Resolving surface chemical states in XPS analysis of first row transition metals, oxides and hydroxides: Cr, Mn, Fe Co and Ni. *Appl. Surf. Sci.* **2011**, *257*, 2717−2730.

(24) Tao, J. G.; Pan, J. S.; Huan, C. H. A.; Zhang, Z.; Chai, J. W.; Wang, S. J. Origin of XPS binding energy shifts in Ni clusters and atoms on rutile TiO2 surfaces. *Surf. Sci.* **2008**, *602*, 2769−2773.

(25) Lei, H.; Song, Z.; Tan, D.; Bao, X.; Mu, X.; Zong, B.; Min, E. Preparation of novel Raney-Ni catalysts and characterization by XRD, SEM and XPS. *Appl. Catal., A* **2001**, *214*, 69−76.

https://doi.org/10.1021/acsomega.2c04354
ACS Omega 2022, 7, 41013−41020